Short-Term Moderately Elevated Intraocular Pressure Is Associated With Elevated Scotopic Electroretinogram Responses

Vivian Choh,[1] Akshay Gurdita,[2] Bingyao Tan,[2] Ratna C. Prasad,[3] Kostadinka Bizheva,[1,2] and Karen M. Joos[3]

[1]School of Optometry and Vision Science, University of Waterloo, Waterloo, Ontario, Canada
[2]Department of Physics and Astronomy, University of Waterloo, Waterloo, Ontario, Canada
[3]Vanderbilt Eye Institute, Vanderbilt University, Nashville, Tennessee, United States

Correspondence: Vivian Choh, 200 University Ave West, University of Waterloo, Waterloo, ON N2L 3G1, Canada;
vchoh@uwaterloo.ca.

Submitted: November 30, 2015
Accepted: March 7, 2016

Citation: Choh V, Gurdita A, Tan B, Prasad RC, Bizheva K, Joos KM. Short-term moderately elevated intraocular pressure is associated with elevated scotopic electroretinogram responses. *Invest Ophthalmol Vis Sci*. 2016;57:2140–2151. DOI:10.1167/iovs.15-18770

Purpose. Moderately elevated intraocular pressure (IOP) is a risk factor for open-angle glaucoma. Some patients suffer glaucoma despite clinically measured normal IOPs. Fluctuations in IOP may have a significant role since IOPs are higher during sleep and inversion activities. Controlled transient elevations of IOPs in rats over time lead to optic nerve structural changes that are similar to the early changes observed in constant chronic models of glaucoma. Because early intervention decreases glaucoma progression, this study was done to determine if early physiological changes to the retina could be detected with noninvasive electrophysiological and optical imaging tests during moderately elevated IOP.

Methods. Intraocular pressures were raised to moderately high levels (35 mm Hg) in one eye of Sprague-Dawley rats while the other (control) eye was untreated. One group of rats underwent scotopic threshold response (STR) and electroretinogram (ERG) testing, while another 3 groups underwent optical coherence tomography (OCT) imaging, Western blot, or histologic evaluation.

Results. The amplitudes of the STR and ERG responses in eyes with moderately elevated IOPs were enhanced compared to the values before IOP elevation, and compared to untreated contralateral eyes. Structural changes to the optic nerve also occurred during IOP elevation.

Conclusions. Although ischemic IOP elevations are well-known to globally reduce components of the scotopic ERG, acute elevation in rats to levels often observed in untreated glaucoma patients caused an increase in these parameters. Further exploration of these phenomena may be helpful in better understanding the mechanisms mediating early retinal changes during fluctuating or chronically elevated IOP.

Keywords: intraocular pressure, scotopic threshold response, ultrahigh-resolution optical coherence tomography, electroretinography

Glaucoma is a chronic disease that is characterized by progressive degeneration of the retinal ganglion cell (RGC) axons within the optic nerve resulting in loss of RGCs and eventually blindness. It is the second leading cause of blindness worldwide, with an estimate of 64.3 million people between the ages of 40 to 80 years affected in 2013, 76.7 million by 2020, and 111.8 million in 2040.[1] According to a 2008 to 2009 survey by Statistics Canada, more than 400,000 people over the age of 45 in Canada have glaucoma.[2] Currently, there is no cure for glaucoma; patients can be treated only with medications or surgery to slow the progression of the disease. Therefore, early detection and early treatment are essential for managing the disease. High Intraocular pressure (IOP) remains a risk factor for open-angle glaucoma (OAG),[3–6] and, therefore, a target for early treatment.

However, a confounding factor is that some patients acquire glaucoma even when their IOPs are normal (IOP $<$ 21 mm Hg) during clinic examinations. Fluctuations in IOP may have a role in the development of glaucoma since multiple studies have demonstrated nocturnal IOP elevation[6–9] or elevations with inversion activities.[10,11] Retinal changes evoked by chronic and acute models of IOP elevation are detectable using various components of the scotopic electroretinogram (ERG).[12–15] The information collected with full-field flash ERGs typically pertains to the photoreceptor and inner nuclear layer cell function. However, components of the scotopic ERG have been shown to reflect proximal retinal functions, including the negative and positive responses to very dim (typically near rod threshold) light stimuli that are too dim to elicit the b-wave; these components are conventionally called scotopic threshold responses (STRs).[16,17]

Joos et al.[18] demonstrated that controlled transient elevations of IOP in rats led to structural changes in the optic nerve that are similar to the early damage observed in chronic glaucoma models but no information about retinal function was available. The present study was done to determine whether acute moderate increases in IOP can lead to glaucomatous damage and whether early changes in retinal

Investigative Ophthalmology & Visual Science

Table 1. Summary of Treatment Details and Targeted IOP

Group	Procedure	Sample Size	Targeted IOP, mm Hg
I	STR/ERG	7	35
II	OCT	6	35
III	Histology	6	35
IV	Western blots	4	35

function can be detected using various components of the scotopic ERG.

Materials and Methods

All procedures in this study were conducted in accordance with the Guidelines of the Canadian Council on Animal Care and conform to the ARVO Statement for the Use of Animals in Ophthalmic and Vision Research. All protocols were approved by the University of Waterloo Animal Care Committee and/or the Institutional Animal Care and Use Committee (Vanderbilt University).

Animals and Anesthesia

Male Sprague-Dawley rats (11 weeks old, approximately 300 g) were obtained from Harlan Labs (Indianapolis, Indiana) and were fed ad libitum. The rats were subjected to a 12-hour light:12-hour dark cycle (maximum 257 lux for 3.5 hours a day) in the housing facility, for the duration of the study, and 1 week before the start of all experiments. Electrophysiological and morphologic tests were done in separate measurement sessions (Table 1): binocular STR and ERG ($n = 7$, Group I) recordings were collected during the first IOP elevation session, and sequential monocular ultrahigh resolution optical coherence tomogram (UHR-OCT) recordings ($n = 6$, Group II) were collected after two previous IOP elevation sessions, 2 days after the initial IOP elevation. Another group of rats underwent the same IOP-raising protocol as the rats used for OCT imaging, and their retinas were harvested either for histologic ($n = 6$, Group III) or for Western blot ($n = 4$, Group IV) analysis.

All rats initially were anesthetized with 2.5% isoflurane in oxygen and maintained with approximately 2% isoflurane in oxygen. The body temperatures of the rats were maintained using heated platforms during anesthesia. Temperatures were monitored using a consumer digital thermometer placed under the abdomen, and breathing rate was assessed every 15 minutes.

For all in vivo procedures, one drop 0.5% proparacaine hydrochloride (Alcaine, topical anaesthetic, #1001600; Alcon, Mississauga, ON, Canada) was applied to the eyes, followed by one drop of 0.5% tropicamide (pupillary dilator; Alcon). The rat corneas were lubricated with artificial tears throughout the duration of the experiments to ensure that the corneas stayed hydrated. Injections of 5 mL sterile saline (0.9% wt/vol NaCl in water) were administered subcutaneously approximately every 1.5 hours during the anesthesia to ensure proper hydration of the animals during the experimental procedures. Although isoflurane is known to reduce the electrophysiological responses when compared to ketamine:xylazine, Liu et al.[19] recently confirmed that it is possible to evoke STRs using isoflurane.

Raised IOP Protocol

Intraocular pressure was raised in one eye by placing an adjustable ligature around the eye anterior to the equator for 1 hour for each procedure.[18] The adjustable ligature consists of a 12-cm length of a medium-size vascular loop (Sentinal Loops; Sherwood-Davis and Geck, St. Louis, MO, USA) measuring 2.5 mm wide and 1.3 mm thick, which was inserted within plastic tubing with 3-mm internal diameter and 1.5-cm length. A light coating of silicone oil was applied to the vascular loop as needed to permit easy adjustment of the tubing and to produce the desired IOP elevation. Additional topical 0.5% proparacaine hydrochloride was applied to the right eye every 20 minutes while the ligature was in place. The targeted IOP was 35 mm Hg to represent an elevated but nonischemic level (Table 1). In the rat, an elevated IOP of 35 mm Hg is associated with an estimated 10% reduction in retinal blood flow, but not with a significant reduction in vessel diameter.[20] The fellow control eye for all rats was left untreated. The IOPs were measured using a rebound tonometer (Icare Tonolab; Icare Finland Oy, Helsinki, Finland). Intraocular pressure was measured using the mean of 5 readings, which reported the best reproducibility indicator (Table 2). Intraocular pressures were monitored throughout the entire experiment and the loop adjusted when necessary.

Table 2. IOP Values Attained for Each Procedure

Experiment	IOP Procedure	IOP ± SD, mm Hg	
		Treated Eye	Control Eye
STR/ERG	Pre	12.4 ± 1.5	13.1 ± 1.9
	During	39.7 ± 4.2	10.6 ± 1.1
	Post	8.9 ± 0.7	9.7 ± 0.8
OCT	Pre	9.1 ± 1.4	9.4 ± 0.8
	During	32.1 ± 6.5	10.9 ± 1.3
	Post	6.3 ± 0.5	8.9 ± 1.7

STRs and ERGs

Before electrophysiological testing, the animals were dark-adapted for at least 12 hours before being transferred in light-proof boxes to the appropriate procedure room. All preparations were done under red illumination (631 nm, <10.9 lux). Anesthetized rats were placed onto a water-heated platform maintained at 38°C (TP650, HHP05; Gaymar, Orchard Park, NY, USA), located in a large box built for dark-adapting animals. The head of the rat was placed into a custom-made head holder and held in place using Velcro straps. A nose cone attached to the head holder allowed continuous delivery of the isoflurane anesthetic to the rats while they underwent the STR and ERG recording procedures.

One drop of artificial tears (Refresh Tears; Alcon) was administered to each eye before placement of a custom-made monopolar silver–silver chloride circular loop electrode onto the limbus of each eye. Reference electrodes were placed under the skin just above the ears[21] such that the tip of electrode was approximately 2.5 mm away from the lateral canthi of each eye. The ground electrode was placed at the back of the head. A commercial handheld Ganzfeld stimulator (Espion Colorburst; Diagnosys LLC, Lowell, MA, USA) was placed immediately in front of each eye.

Binocular STRs and ERGs were recorded before increasing the IOP, 45 to 50 minutes into the 1-hour raised IOP procedure, and 30 minutes after the loop removal. Scotopic threshold responses were recorded from 7 rats over 500 ms at a 1 kHz sampling rate with the system's built-in filter of 0.3 to 30 Hz, similar to the protocol of Bui and Fortune.[22] Following 10 minutes in the light-proof box, the rats were exposed to binocular uniform flashes of light with step-wise increases in luminance. Twelve luminance levels were used for the STR

Investigative Ophthalmology & Visual Science

recordings (–6.64 log cd·s/m^2 to –3.04 log cd·s/m^2), with each luminance level consisting of 60 one-millisecond white flashes, separated by a 2-second dark interval. Scotopic threshold response protocols were identical for rats, regardless of the targeted IOP. Electroretinograms were recorded from the same rats that underwent STR recordings ($n = 7$) at a 2 kHz sampling rate with the built-in filter set to 0.3 to 500 Hz immediately following the STR luminance series, that is, within the 1-hour of IOP elevation. The ERG luminance series consisted of 14 single 1 ms white flashes (–2.79 log cd·s/m^2 to 1.46 log cd·s/m^2) that were separated by progressively longer dark intervals (10–95 seconds).

Ultrahigh-Resolution OCT (UHR-OCT)

Morphologic images of the retina were acquired in vivo ($n = 6$ rats) using a research-grade UHR-OCT system designed and built by our group specifically for imaging of rodent retinas. In brief, the UHR-OCT system operates in the 1060 nm spectral range (Superlum Ltd., $\lambda_c = 1020$ nm, $\Delta\lambda = 110$ nm, $P_{out} = 10$ mW). The UHR-OCT imaging probe consists of 3 broadband NIR achromat doublet lenses ($f_1 = 10$ mm, $Ø_1 = 6$ mm, $f_2 = 60$ mm, $Ø_2 = 25$ mm, $f_3 = 30$ mm, and $Ø_3 = 25$ mm; Edmund Optics, Barrington, NJ, USA) and a pair of galvanometric scanners (Cambridge Technologies, Bedford, MA, USA), and is designed to deliver a collimated infrared beam with 1.5-mm diameter and optical power of 1.7 mW to the rat cornea, thus providing approximately 3 μm axial and better than 5 μm lateral resolution in the rat retina at an imaging rate of 47,000 lines/second.[23] The digital axial resolution is 1.6 μm. For the UHR-OCT imaging procedure, the rats were placed onto a heated stage. The treated and untreated control eyes were imaged sequentially. The imaged eye was kept open using a custom-made lid retractor and artificial tears were administered every few minutes to keep the cornea hydrated. Three-dimensional (3D) stacks of cross-sectional OCT images (1024 lines/frame × 1024 pixels/line) of the retina were acquired from an approximately 2 × 2 mm area in the retina centered at the optic nerve head (ONH). Preloop UHR-OCT images were collected monocularly on the future control eye, followed by recordings of the future treated eye. The IOP was then raised in the treated eye and images from this eye were collected 30 minutes into the raised IOP procedure. Recordings for the control eye were collected immediately thereafter, while the loop still was on the treated eye. At the end of the 1-hour raised IOP procedure, the loop was removed and recordings for the control and then the treated eyes were likewise sequentially collected 30 minutes after the removal of the loop.

Histology and Immunocytochemistry

Five days after the initial IOP elevation, the rats were killed, and then perfused with heparinized saline followed by 4% (wt/vol) paraformaldehyde (#158127; Sigma-Aldrich Corp., St. Louis, MO, USA) in PBS. Eyes were enucleated and the orientation of the globe was indicated using a suture at the nasal limbus. The globes were postfixed for 2 days in 4% (wt/vol) paraformaldehyde in PBS and then briefly stored in PBS.

The globes that were used for histologic analysis were embedded in paraffin. Eyes from all 6 rats were serially sectioned in the sagittal plane passing through the optic nerve at a thickness of 6 μm. Representative sections on either side of the optic nerve were stained with hematoxylin (SL90; Statlab, Lewisville, TX, USA) and eosin (C.I. 45380; EMS, Hatfield, PA, USA) for light microscopy. On other sections, also from either side of the optic nerve, antigen retrieval was performed using boiling citric acid treatment (1.8 mM citric acid, 8.2 mM sodium citrate) for 10 minutes. Sections were allowed to cool at room temperature for 30 minutes. Retinal sections were treated with 3% (vol/vol) hydrogen peroxide (20 minutes) to quench endogenous peroxidase and then additionally quenched in 0.3% (vol/vol) sodium borohydride (# S678-10; Fisher Scientific, Pittsburgh, PA, USA) in PBS for 30 minutes before placing them in 5% (vol/vol) normal goat serum in PBS (1 hour) to prevent nonspecific binding. Two primary antibodies were used: rabbit polyclonal anti-poly (ADP-ribose) polymerase (PARP) p85 fragment (1:100; #G7341, Promega, Madison, WI, USA) to evaluate for apoptosis, and rabbit monoclonal anti–microtubule-associated protein light chain 3 (anti-LC3A/B [N-terminus]; 1:100; #MABC176, Millipore, Billerica, MA, USA) to evaluate for autophagy. All sections were incubated with primary antibody overnight at 4°C before incubation with Cy3-conjugated AffiniPure Goat Anti-Rabbit IgG (1:200; #111-165-144, H+L chains; Jackson ImmunoResearch Laboratories, Inc., West Grove, PA, USA) at room temperature for 1 hour. Sections then were rinsed in water and allowed to air dry before mounting with Aqua-Poly/Mount (#18606-20; Polysciences, Inc., Warrington, PA, USA) under a coverslip. Retinal sections were examined using a Zeiss LSM510 Meta confocal microscope (Carl Zeiss Meditec, Jena, Germany).

Retinas ($n = 4$ pairs, with one retina per lane) used for Western blot analysis were sonicated (Sonic 300 V/T ultra-sonic dismembrator; Imaging Products International, Simi Valley, CA, USA) in ice-cold radio-immunoprecipitation assay (RIPA) lysis buffer (R0278, Sigma-Aldrich Corp.) containing protease (P8340; Sigma-Aldrich Corp.) and phosphatase (#P2850 and #P5726; Sigma-Aldrich Corp.) inhibitor cocktails. The homogenate was centrifuged (8000 × g, 10 minutes, 4°C) and the supernatant was transferred. Protein concentrations were measured (SmartSpec Plus Spectrophotometer; #1702525; Bio-Rad for Spectroscopy, Philadelphia, PA, USA) and equalized before adding 2× Laemmli Sample buffer (#SC 286962; Santa Cruz Biotechnology, Dallas, TX, USA) to each sample and loading onto 12% and 7.5% SDS-PAGE precast gels (#456-1044 and #456-1024, Bio-Rad Mini-Protein TGX Precast gels; Bio-Rad, Life Science Research, Hercules, CA, USA; for anti-LC3A/B and PARP p85 fragment labeling, respectively). Samples were transferred to 0.2 μm nitrocellulose membranes (#9004-70-0; Bio-Rad, Life Science Research) and membranes were incubated overnight with primary antibodies to LC3A/B (anti-LC3A/B, clone EP1983Y, rabbit monoclonal, #MABC176; Millipore) or to PARP P85 fragment (anti-PARP p85 fragment, #G7341, anti-rabbit; Promega), both at 1:2000 concentrations. Membranes were incubated in horseradish peroxidase (HRP)–conjugated goat anti-rabbit IgG secondary antibody (1:5000, 1.5 hours, RT; #W4011; Promega) and proteins were visualized using Amersham ECL Western Blotting Chemiluminescence Detection Reagent (#RPN2106; GE Healthcare, Pittsburg, PA, USA) and photographed. Membranes then were stripped (Restore Western Blot Stripping Buffer, #21059; Thermo Fisher Scientific, Rockford, IL, USA) before immunoblotting for β-actin as a loading control (primary: β-actin, 1:2000; #8H10D10; Cell Signalling, Boston, MA, USA; secondary: HRP-conjugated goat anti-mouse secondary antibody, 1:5000, 1.5 hours, RT, #W4021; Promega). Densitometry analysis of the immunoblots was done using ImageJ software (http://imagej.nih.gov/ij/; provided in the public domain by the National Institutes of Health, Bethesda, MD, USA), and protein levels were normalized against β-actin levels.

Analysis of STR and ERG Data

The positive STR (pSTR) amplitude was considered to be the peak positive change in voltage from the baseline voltage to the first peak in the STR recording. Since we were interested in

Investigative Ophthalmology & Visual Science

Figure 1. Representative ONH-centered B-scan demonstrating the method used to determine xBMO depth. Each xBMO depth (*blue line*) was determined relative to the orthogonal plane connecting Bruch's membrane/RPE interfaces at the edges of the cross-sectional image (*red line*) and averaged. *Vertical* and *horizontal scale bars*: 100 μm.

RGC function, we examined pSTRs, which are considered to involve RGCs.[24,25] We did not examine negative STRs (nSTRs), since they were not consistently present in the records and more likely involve amacrine cells.[24,25] An absence of nSTRs also has been observed in other rodent studies.[19,26] For ERG traces, a-wave amplitudes were measured as the maximum change in voltage from the baseline to the first negative trough, while b-wave amplitudes were measured as the change in voltage from the a-wave to the peak positive change following the a-wave. For all three measures (pSTR, a- and b-waves), implicit times were measured from the light stimulus onset to the peak amplitude. A few of the ERG recordings were noticeably translated by the recording system, where the beginning of the waveforms were not recorded until just before the a-wave appeared, indicating a failure in the trigger timing of the recording software. However, the intervals between the a- and b-waves, as well as their amplitudes were unaffected and, therefore, only the implicit times for ERGs that were improperly recorded were adjusted. For each shifted ERG recording, the a-wave implicit time was matched to the average of those recordings at the same luminance level, same IOP state, and same eye ($n = 6$). The rest of the waveform was shifted by the same correction factor. Oscillatory potentials (OPs) were isolated from ERG recordings by applying a customized SigmaPlot bandpass filter (100–300 Hz). For each recording, the root mean square (RMS) value for the OP amplitudes were determined for a 60 ms window starting from the a-wave implicit time.

Analysis of UHR-OCT Data

Cross-sectional images of the retina were generated from the raw morphologic UHR-OCT data using a custom MATLAB-based software (Mathworks, Natlick, MA, USA). Three-dimensional reconstruction of the cross-sectional images (Amira; FEI Company, Hillsboro, OR, USA) was used to generate a 3D view of the imaged retinal area at and around the ONH. The unique pattern of the surface retinal blood vessels was used as a marker to align all 3D image data sets acquired before, during, and after IOP elevation to allow for direct comparison of the morphologic changes in the rat retina at all time points of the study. By collapsing the 3D image to a 2D en face projection image, and fitting the end points of the Bruch's membrane at the ONH with an ellipse, we were able to determine the center of the ONH in a consistent manner for image data sets acquired at different time points of our study. For our analysis, we considered the end points of the Bruch's membrane to be the points at which the Bruch's membrane/RPE interface terminates on either side of the optic nerve in a cross-sectional image.[27,28] Once the ONH center was determined, the B-scan passing through it was used for the calculation of the cross-sectional Bruch's membrane opening (xBMO) depth, defined here as the average depth orthogonal to the plane connecting Bruch's membrane/RPE interfaces at the edges of the cross-sectional image (Fig. 1). Cross-sectional BMO depths were analyzed as a function of loop wear by the same two experimenters for all images.

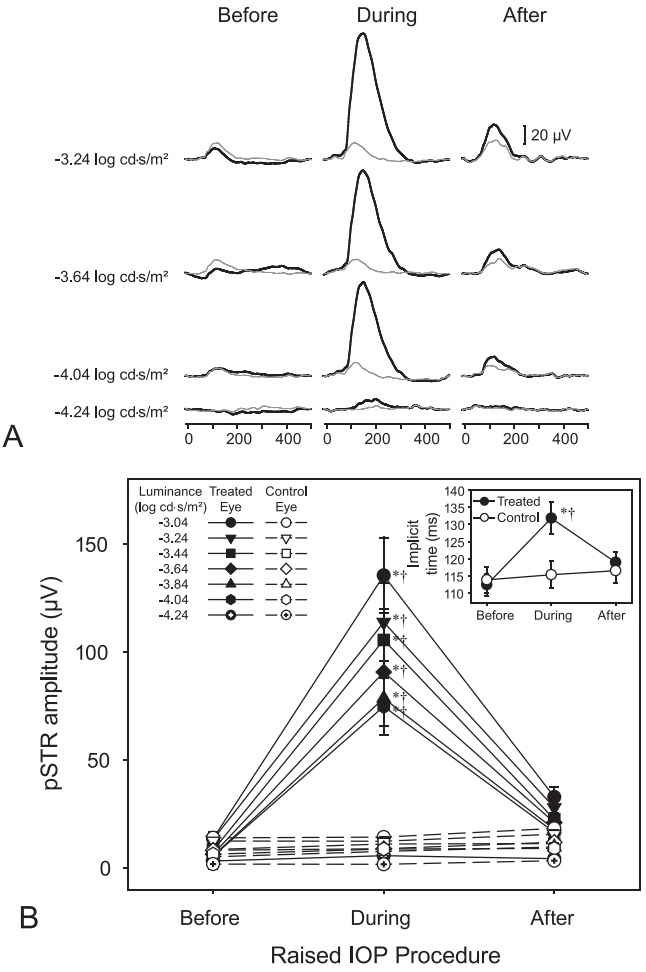

Figure 2. (**A**) Sample STRs from a treated eye (*thick black lines*) and its control eye (*thin gray lines*) before, during, and following 35 mm Hg IOP elevation. (**B**) Mean pSTR amplitudes ± SE of STRs for the treated eyes (*filled symbols*) and control eyes (*empty symbols*) during the various stages of loop wear. Scotopic threshold responses were evident at flash intensities greater than −4.24 log cd·s/m² up to −3.04 log cd·s/m². *Inset*: Mean implicit times ± SE of the treated (*filled symbols*) and control (*empty symbols*) eyes during the various stages of loop wear. *Significant differences ($P < 0.05$) relative to the respective preloop and luminance condition. †Differences ($P < 0.05$) between eyes for the specific loop and luminance condition. Please refer to text for overall and all other comparisons.

Statistical Analysis

For all data, 2-way repeated-measures ANOVA (Statistica 8.0, Statsoft, Boston, MA, USA) was used to determine differences in the amplitudes, implicit times, and xBMO depths, with the eye used (treated versus control) as one factor and the loop condition (pre-, during, and postloop wear) as the second factor. Interaction between the two main effects also was tested.

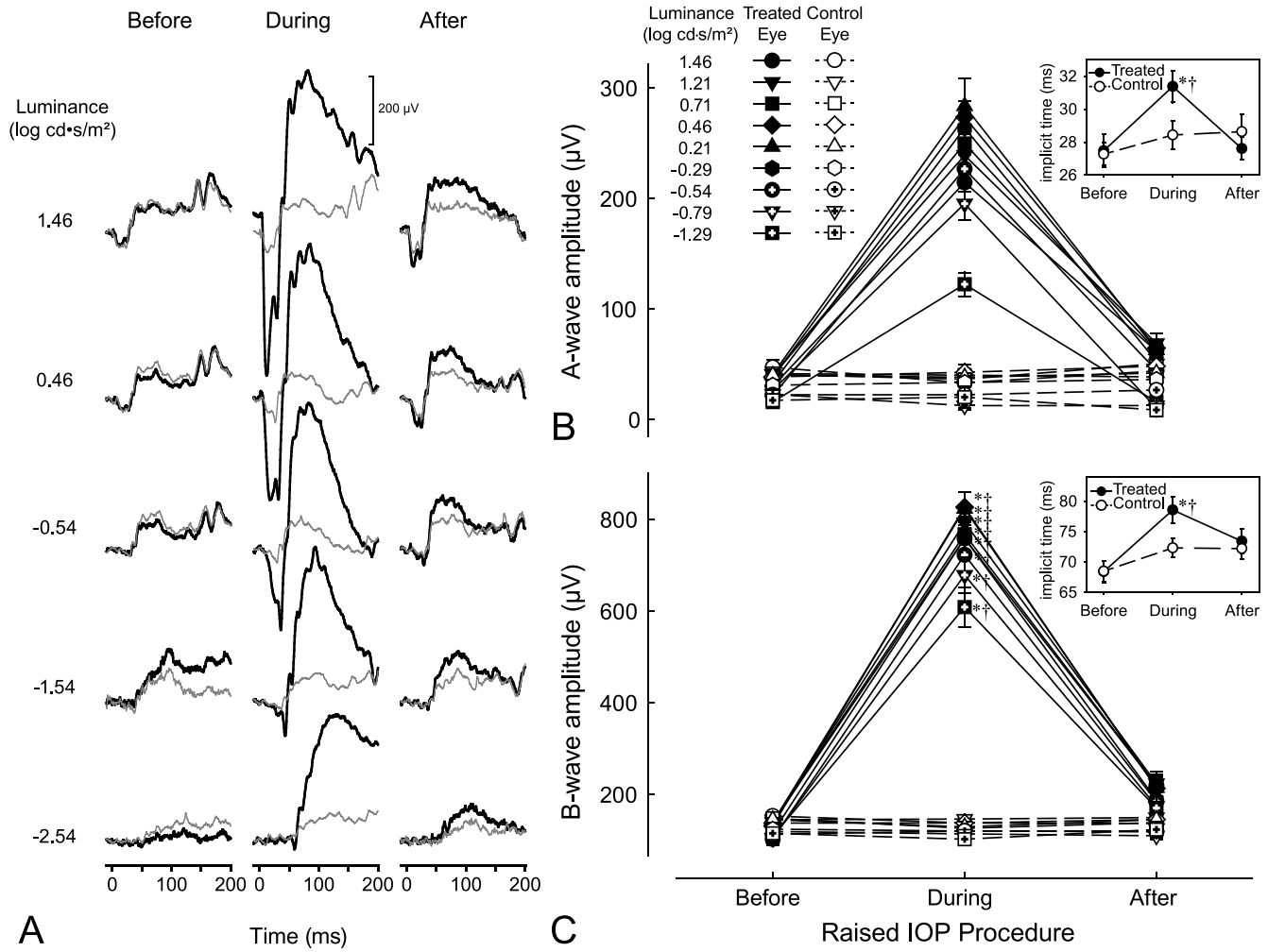

Figure 3. (**A**) Sample ERGs from a treated eye (*thick black lines*) and its control eye (*thin gray lines*) before, during, and following 35 mm Hg IOP elevation of the treated eye. Enhanced responses occur with IOP elevation. (**B**) Mean peak amplitudes ± SE of the a-waves and (**C**) b-waves for the treated eyes (*filled symbols*) and control eyes (*empty symbols*) during the various stages of loop wear. *Inset*: Mean (**B**) a-wave, and (**C**) b-wave implicit times ± SE of the treated (*filled symbols*) and control (*empty symbols*) eyes during the various stages of loop wear. *Significant differences ($P < 0.05$) relative to the respective preloop and luminance condition. †Significant differences ($P < 0.05$) between eyes for the specific loop and luminance condition. Please refer to text for overall and all other comparisons.

Greenhouse-Geisser corrections were used for epsilon values less than or equal to 0.75. Bonferroni-corrected multiple comparison tests were used post hoc to determine any differences between the loop conditions. For all tests, differences were considered significant for $P < 0.05$. All means are reported with the SD unless otherwise noted.

Results

STR and ERG Amplitudes

Peak amplitudes and implicit times were measureable from the STR recordings (Fig. 2A) elicited with luminance levels greater than –4.24 log cd·s/m^2; responses were most consistently observed for pSTRs elicited by the highest stimulus luminance (–3.04 log cd·s/m^2). Although there were exceptions among the individual eyes, higher stimulus intensities were, on average, associated with higher pSTR amplitudes ($P < 0.0001$).

Loop-associated elevations in pSTR amplitudes were consistently observed at luminances greater than –4.24 log cd·s/m^2. Increasing the IOP led to enhancement of the pSTR peak amplitudes (Figs. 2A, 2B). In treated eyes, the mean pSTR amplitudes (±S.D.) during loop wear (86.4 ± 51.9 μV) were significantly higher ($P < 0.0001$) than those before loop wear (7.9 ± 5.1 μV) and higher ($P < 0.0001$) than those after loop removal (20.5 ± 11.3 μV). Positive STR amplitudes before and after loop wear were not significantly different ($P = 1.000$). No differences in pSTR amplitudes were detected in the control (untreated eyes) as a function of loop wear ($P = 1.000$ for all comparisons), indicating an absence of an IOP-associated fellow-eye effect. Pre- and postloop pSTR amplitudes were not statistically different between the treated and control eyes before loop placement (7.9 ± 5.1 vs. 8.1 ± 6.1 μV, respectively, $P = 1.000$) or postloop placement (20.5 ± 11.3 vs. 11.3 ± 6.4 μV, respectively, $P = 1.000$). However, during loop wear, the pSTR amplitudes were higher in the treated eyes than in the control eyes (86.4 ± 51.9 vs. 9.3 ± 5.2 μV, respectively; $P < 0.0001$; Figs. 2A, 2B). In the treated eyes, implicit times during loop wear (131.8 ± 16.6 ms) were longer than those during the pre- (112.4 ± 13.4 ms; $P < 0.0001$) or postloop (118.9 ± 16.2 ms; $P < 0.0001$) conditions (Fig. 2B, inset). Moreover, differences were detected between the preloop and postloop conditions in these treated eyes ($P = 0.0299$). Within the control eyes, no implicit time differences were detected as a function of

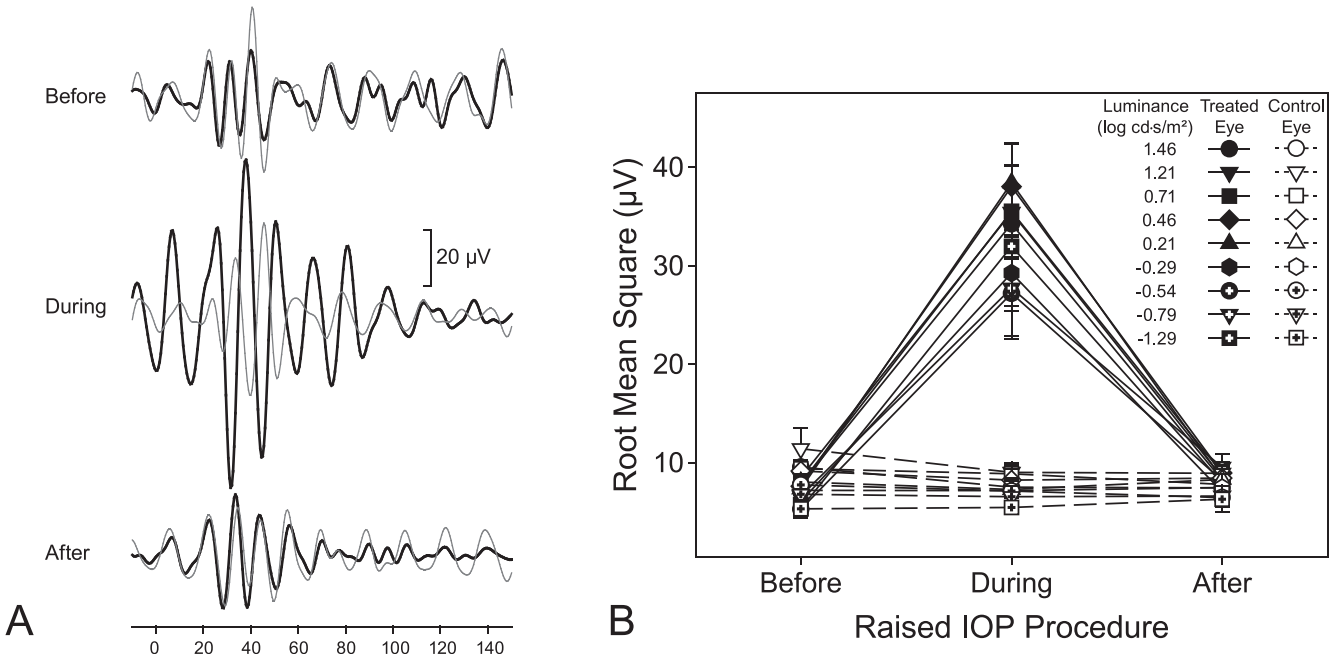

Figure 4. (**A**) Sample OPs (isolated via a 100–300 Hz bandpass filter) from a treated (*thick black lines*) and its control (*thin gray line*) eye before, during, and following 35 mm Hg IOP elevation of the treated eye at a luminance of 2.88 log cd·s/m^2. (**B**) Mean RMS values ± SE for OPs before, during, and following 35 mm Hg IOP elevation of the treated (*filled symbols*) and control (*empty symbols*) eyes. Please refer to text for comparisons.

loop wear ($P = 1.000$ for all comparisons). Like the patterns observed for the pSTR amplitudes, the implicit times were similar between the treated and control eyes for the preloop (112.4 ± 13.4 vs. 113.8 ± 14.9 ms, respectively, $P = 1.000$) and postloop (118.9 ± 16.2 vs. 116.5 ± 16.5 ms, respectively; $P = 1.000$) time-points. However, implicit times were longer for treated eyes than control eyes (131.8 ± 16.8 vs. 115.3 ± 19.5 ms, respectively; $P < 0.0001$) during loop wear.

All ERG waveforms consistently showed a- and b-wave amplitudes and OPs on the rise of the b-wave at luminances greater than –0.54 log cd·s/m^2 (Fig. 3A). Like the pSTRs, amplitudes generally were greater with higher luminance levels ($P = 0.0011$) and during elevated IOP (Figs. 3A–C). Specifically, a-wave amplitudes during loop wear (–228.4 ± 29.7 μV) were significantly greater in magnitude than those during the preloop (–31.4 ± 9.9 μV; $P < 0.0001$) and postloop (–49.0 ± 12.6 μV; $P < 0.0001$) conditions (Fig. 3B). Similarly, b-wave amplitudes during loop wear (747.9 ± 74.5 μV) were significantly greater than those before (123.8 ± 29.0 μV; $P < 0.0001$) and following (200.0 ± 56.0 μV; $P < 0.0001$) loop wear (Fig. 3C). In the treated eyes, there were no differences between the pre- and postloop conditions in the a-wave amplitudes ($P = 0.4602$), but b-waves amplitudes during postloop condition were greater than those before loop wear (compare 200.0 ± 56.0 vs. 123.8 ± 29.0 μV, respectively; $P = 0.0081$). The enhanced a-wave and b-wave amplitudes in the treated eyes were significantly greater than those in the control eyes ($P < 0.0001$ for both; Figs. 3B, 3C). A- and b-wave amplitudes in control eyes did not differ as a function of contralateral loop wear ($P = 1.000$ for both ERG components). A-wave implicit times also were longer during loop wear (31.6 ± 2.4 ms) than those during preloop (27.8 ± 2.6 ms; $P < 0.0001$) and postloop (27.8 ± 1.8 ms; $P < 0.0001$) conditions (Fig. 3B, inset). Similarly, b-wave implicit times were also longer during loop wear (78.9 ± 5.6 ms) than those during pre- (68.9 ± 5.6 ms; $P < 0.0001$) and postloop (73.5 ± 5.2 ms, $P = 0.0223$) conditions (Fig. 3C, inset). There were no differences between pre- and postloop a-wave implicit times ($P = 1.000$), however, b-wave implicit times for postloop conditions were longer than those for preloop (73.5 ± 5.2 vs. 68.9 ± 5.6 ms respectively; $P = 0.0247$) conditions. Implicit times during loop wear for a- and b-waves were greater than control eyes (31.6 ± 2.4 vs. 28.5 ± 2.0 ms, $P = 0.0008$ for a-waves; 78.9 ± 5.2 vs. 72.5 ± 3.8 ms, $P = 0.0054$ for b-waves; insets of 3B and 3C). For both a- and b-wave implicit times, control eyes did not change for all comparisons ($P > 0.1275$). Oscillatory potential amplitudes were greater in the treated eyes during loop wear (Fig. 4A) and the root mean square values the OPs during IOP elevation (33.1 ± 10.1 μV) increased significantly compared to pre- (7.0 ± 1.3 μV; $P < 0.0001$) and postloop (8.4 ± 2.9 μV; $P < 0.0001$) wear conditions (Fig. 4B). For treated eyes, pre- and post-RMS values did not significantly differ ($P = 1.000$). Root mean square values did not change for control eyes for all loop conditions ($P = 1.000$).

Morphology (Imaging and Histology)

Ultra-high resolution OCT imaging indicated that IOP elevation had an effect on physiological cup morphology; 3-D and 2-D cross-sectional images of the ONH indicated a "backward bowing"[29,30] of the retina (Fig. 5). The xBMOs during IOP

Table 3. Mean BMO Depth Derived From Morphologic OCT Images of Rats In Vivo

	BMO Depth ± SD, μm	
IOP Procedure	**Treated Eye**	**Control Eye**
Pre	59.5 ± 24.9	68.0 ± 38.6
During	147.1 ± 30.3*†	67.3 ± 11.2
Post	80.9 ± 16.1	68.4 ± 19.8

* Significant differences ($P < 0.05$) relative to the respective preloop condition.

† Differences ($P < 0.05$) between eyes for the specific loop condition. For more comparisons, please see text.

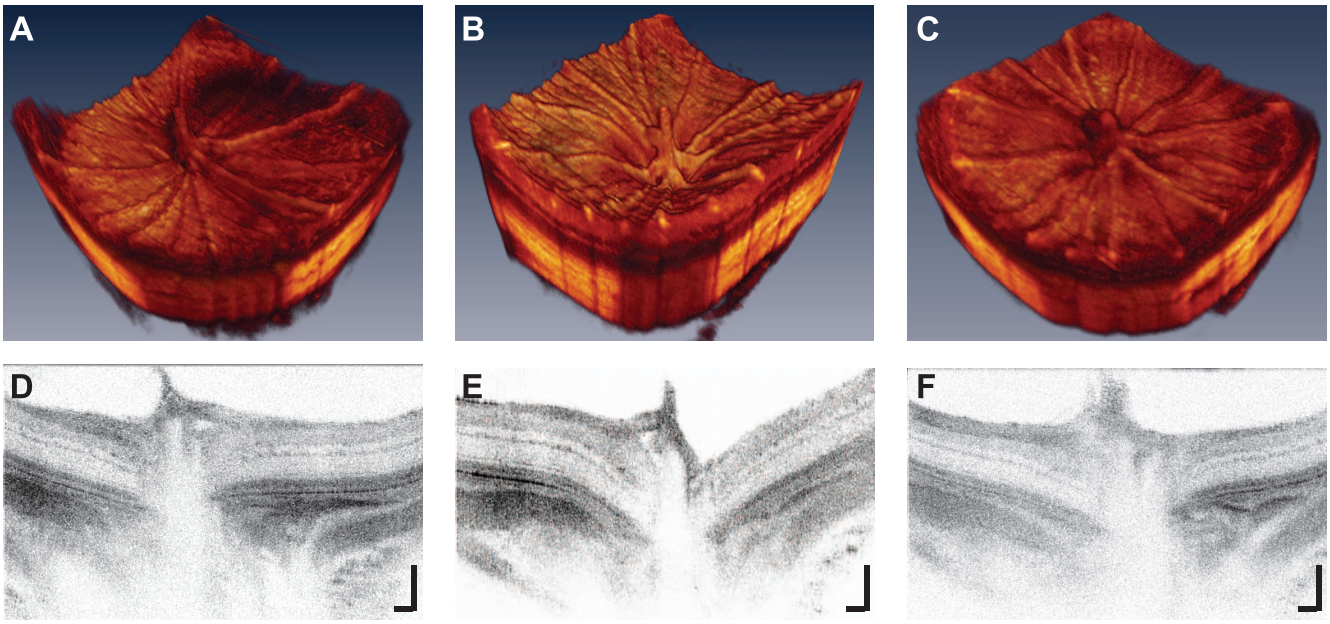

FIGURE 5. Optical coherence tomography images of the treated eye (**A**, **D**) before, (**B**, **E**) during, and (**C**, **F**) following loop wear centered about the ONH. Note "posterior bowing" of the ONH in the (**B**) three dimensional and (**E**) cross-sectional images. *2-D image scale bars*: 100 μm.

elevation (147.1 ± 30.3 μm) were significantly deeper than before loop wear (59.5 ± 25.0 μm, $P = 0.0134$, Table 3), but not significantly deeper compared to postloop wear (80.9 ± 16.1 μm; $P = 0.0701$). However, pre- and postloop xBMO depths for the treated eye also were not significantly different ($P = 1.000$), indicating a partial recovery after 30 minutes of the xBMO depths to their preloop values. The xBMO depths during IOP elevation were greater in the treated eye compared to depths in the control eyes (compare 147.1 ± 30.3 vs. 67.3 ± 11.2 μm, respectively; $P = 0.0238$, Table 3), while preloop xBMO depths between the eyes were similar (treated versus control, 59.5 ± 24.9 vs. 68.0 ± 38.6 μm; $P = 1.000$, respectively). The control eye xBMO depths did not change as a function of contralateral eye loop wear.

Hemotoxylin and eosin (H&E) staining of retinal sections revealed no apparent differences (Figs. 6A, 6B) between the treated and control eyes. An absence of a difference between the eyes also was noted for specific cell death markers in the retinas. While the retinas of the treated and control eyes were moderately labelled with anti-LC3A/B, an autophagy marker, in many of the cells within the ganglion cell layer, and in the inner and the outer plexiform layers, there appeared to be no difference in the intensity or location of labeling between eyes (Figs. 6C, 6D). Similarly, no differences were detected between the control and treated eyes for poly (ADP-ribose) polymerase (PARP) p85 fragment (Figs. 6E, 6F), a marker for apoptosis. Fragment-labeling of PARP p85 was absent in the inner retina of the treated and control eyes, and labeling resembled that of the negative control (Fig. 6G). A positive early glaucoma control for PARP p85 fragment shows that this marker localizes to the cytoplasm of cells in the ganglion cell layer (Fig. 6H; Joos, unpublished data). Thus, the analysis using immunocytochemistry indicated that short-term IOP did not result in apoptosis within 5 days of the initial IOP elevation. Densitometry analysis of Western blots (Fig. 7A) confirmed that there were no differences in the amounts of LC3A ($P = 0.2202$), LC3B ($P = 0.3769$), and PARP p85 fragments ($P = 0.2521$; Fig. 7B) between the eyes.

DISCUSSION

This study was done to determine whether early changes to retinal function in response to acute moderately-raised IOP was detectable electrophysiologically and morphologically. In eyes with IOPs elevated to approximately 35 mm Hg, the pSTR and ERG a-wave and b-wave amplitudes were increased compared to those before loop wear, and also compared to the control eyes (Figs. 2, 3). Other investigators typically show reductions in the ERG and pSTR amplitudes, usually at IOPs greater than 50 mm Hg, with a consistently low amplitude starting at approximately 80 mm Hg and above.[13,14] Our study examined acute, nonischemic moderate levels of IOP that were elevated using a vascular loop, while most other studies use cannulation into either the anterior or vitreous chamber.[14,31] The increase, rather than decrease, in pSTR amplitude that we observed in this experiment is likely related to the moderate level of IOP and cannot be related solely to the use of the vascular loop to increase IOPs, as opposed to IOP elevation based on cannulation or microbead injections. Using the same STR protocols (as Group I, Table 1), pilot data indicated that pSTR amplitudes were unaffected when the loop was on the treated eye without an increase in IOP (Fig. 8A). However, when IOP levels were elevated with the vascular loop to ischemic levels (80 mm Hg), at which blood flow and vessel diameter decrease by 80%,[20] a severe reduction, rather than an increase, in the pSTR amplitudes was observed (Fig. 8B), a finding that is similar to the results presented by Bui et al.,[13] who show an inflection point at 80 mm Hg, IOPs above which result in all ERG components (except for the a-wave) unable to "with-[stand] this pressure level."[13] It also should be noted that in other studies examining the incremental effects of acutely elevated levels of IOPs on the pSTR amplitudes, the data for IOPs at or below 30 mm Hg imply slight increases in pSTR responses[13,14] despite the difference in method of IOP elevation. Given that the rats were anesthetized with ketamine, the increase in the pSTR amplitudes that was observed in these studies suggest that the increase in amplitudes in our study are independent of the anesthetic used. Finally, the different rat strains used in other studies may also be a contributing factor

Investigative Ophthalmology & Visual Science

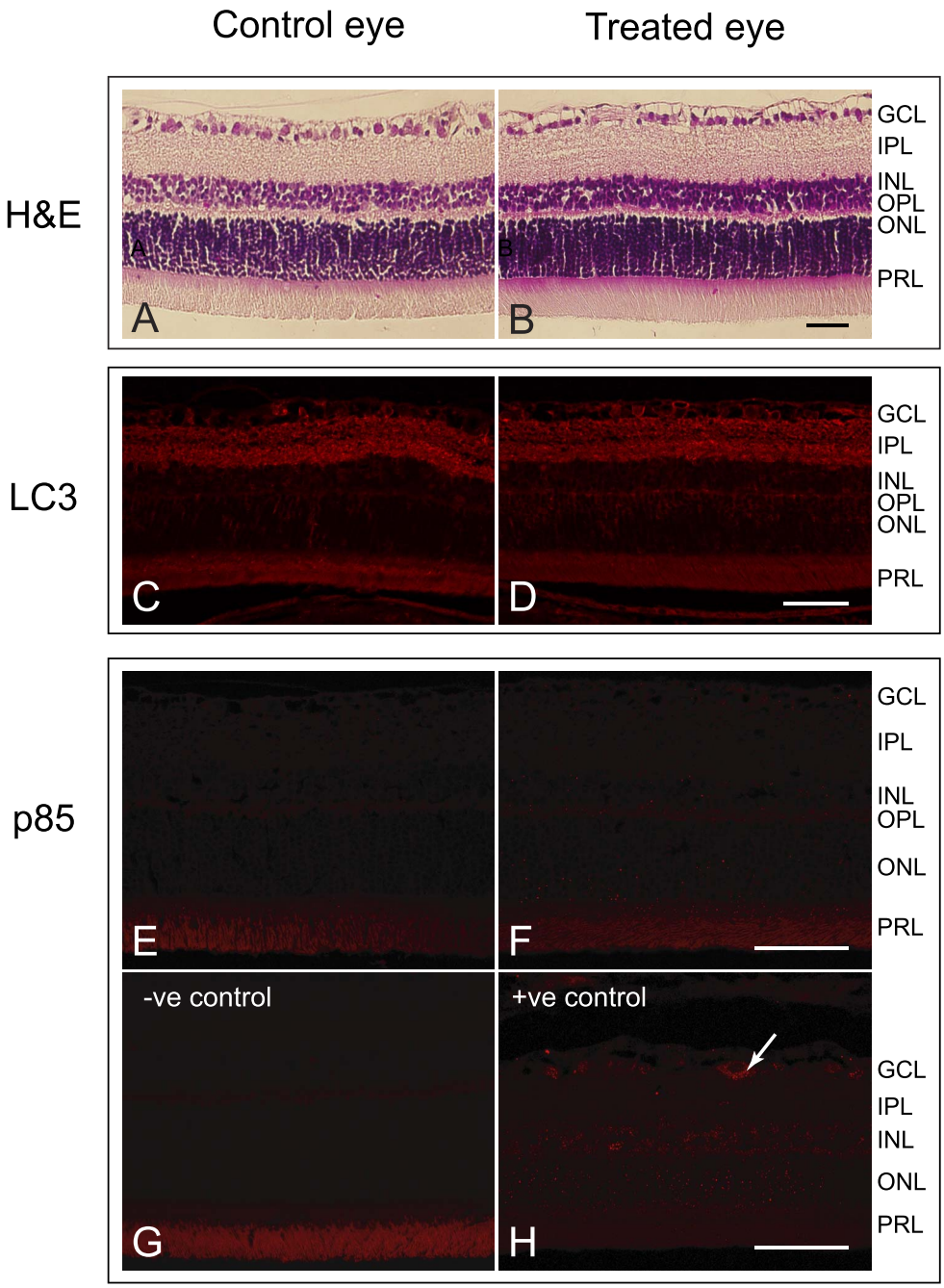

Figure 6. Histologic cross-sectional images of the retina from (**A**) a control and (**B**) a treated eye. No gross differences in the retinas were observed. *Scale bars*: 50 μm. Micrographs of retinas from (**C**) a control and (**D**) a treated eye labeled for LC3A/B. LC3A/B was detected in the GCL, IPL, and OPL. No differences in the labeling were detected. Autofluorescence was present within the photoreceptor layer (PRL) as demonstrated by the primary antibody negative control (not shown). *Scale bar*: 50 μm. Micrographs of retinas from (**E**) a control and (**F**) a treated eye labelled for PARP p85 fragment. Only autofluorescence was detected within the PRL, as demonstrated by the primary antibody negative control (**G**). A positive control from a 6-week intermittently elevated IOP glaucomatous rat (unpublished data from Joos et al.[18]) shows the PARP p85 fragment in the cytoplasm of a cell in the RGC layer (*arrow*) (**H**). *Scale bar*: 50 μm.

when comparing our study to previously published literature.[13,14]

It is possible that using the vascular loop might change the global shape of the eye with backward bowing and, therefore, potentially affect the signals received at the cornea. However, as observed by Westall et al.,[32] reductions rather than the observed increases in ERG amplitudes would be expected for longer eyes, while enhancement of the signal would be expected for shorter eyes. The posterior bowing of the retina observed in our experiments, must be related, at least in part, to the increase in IOP. Backward bowing of the posterior pole following IOP elevation has been known for decades and for a number of structures, including the optic disc in infant humans,[30] the retina in rats,[20] the retinal pigment epithelium/Bruch's membrane[29] in primates, and the lamina cribrosa in primates[27] and humans.[33] While most of these studies involve cannulation of the anterior chamber[20,29,34] or vitreous chamber[33,35] as the means of elevating IOP, Gramlich et al.[36]

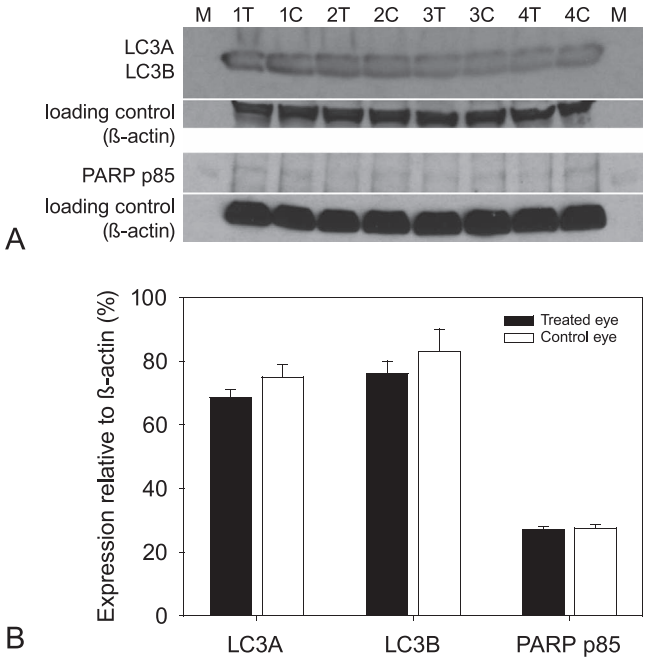

Figure 7. (**A**) Western blots of LC3A/B and PARP p85 fragment in 4 animals after 3 episodes of elevated IOP. β-Actin was used as the loading control for markers. (**B**) Mean expression of the cell markers relative to β-actin for treated (*filled bars*) and control (*empty bars*) eyes. No significant differences were detected between the eyes for each of the markers.

qualitatively showed that posterior bowing deepened with increasing levels of IOP in rats whose IOPs had been raised using a loop around the equator of the eye, and Ivers et al.[37] showed deepening of the anterior lamina cribrosa surface following laser treatment of the trabecular meshwork in rhesus monkeys. The xBMO depth changes observed in our study are comparable to those of the aforementioned investigators. Although morphologic responses were measured in rats with IOPs raised 2× before the final assessment, our acute, moderately-elevated IOP model revealed no changes to cell death marker levels in the treated eyes relative to the control eyes (Figs. 6, 7). This result is consistent with an acute, nonpathologic response, despite IOP elevation for the prior 2 sessions. These markers are important because their presence has been reported in previous investigations that are more chronic in nature.[38] It is probable that additional IOP elevations over longer periods of time would lead to effects on the xBMO depths; however, the finding that the control eye preloop xBMO depths (from eyes that had no IOP elevation) were not different from the treated eye preloop xBMO depths (IOPs had been elevated 2× before the UHR-OCT imaging session; Table 3) would seem to indicate that the eye can tolerate a small number of IOP elevations. Elevation of the a-wave, b-wave, and OPs in the scotopic ERG implies that the outer retina also is affected by moderately elevated IOP. Electrophysiology has demonstrated reduction of these components in animal models with chronic ocular hypertension (OHT) including Swiss mice with histologic abnormalities of rod bipolar and horizontal cells.[39] DBA/2NNia mice with thinning of the ganglion cell layer (GCL), inner plexiform layer (IPL), outer plexiform layer (OPL), and rods,[40] and DBA/2J mice with synaptic abnormalities of outer retinal cells.[41] In humans with advanced glaucoma, reductions in scotopic ERG amplitudes for the a-wave,[42] b-wave,[42,43] and OPs[42,44] have been reported, as well as loss of the positive peak of the STR,[42] and reduced focal ERG amplitudes.[45]

Chen et al.[46] have suggested that a decrease in b-wave ERG amplitudes are indicative of ischemia but supranormal ERGs also are suggestive of pathology, rather than a normal variant.[47] Supranormal scotopic a-wave and b-wave amplitudes with

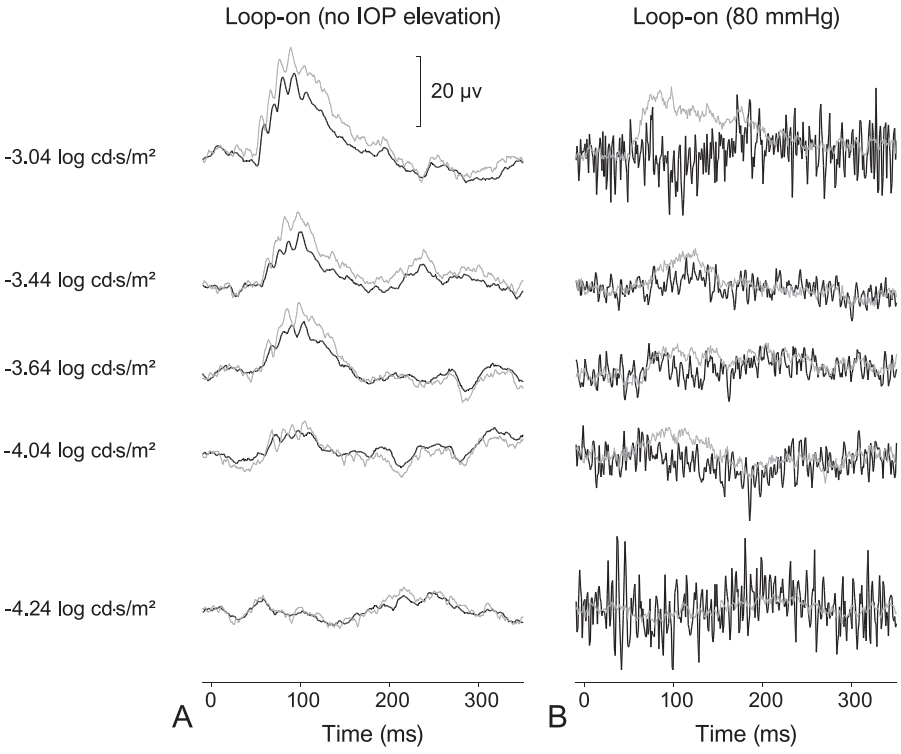

Figure 8. Scotopic threshold responses during loop wear in the treated (*thick black lines*) and control (*thin gray lines*) eyes (**A**) with no increase in IOP (10 mm Hg) and (**B**) at 80 mm Hg.

normal implicit times have been noted in specific conditions, including loss of retinal dopaminergic amacrine cells,[48,49] blockage of retinal dopamine receptors,[50,51] gestational low-level lead exposure in rats[52] and humans,[53] loss of a mitochondrial ATP transporter in *Ant1*$^{-/-}$ mice,[54] and in a microbead occlusion mouse model, with an approximate 20% increase in b-wave amplitude present up to 48 weeks with a 3 to 5 mm Hg mean IOP elevation.[12,55] Supranormal a-wave and b-wave scotopic and photopic ERGs with shortened implicit times also have been found in the Fat-1 mouse with deletion of n-6 and accumulation of n-3 fatty acids in the retina,[56] and amplitudes were likewise increased with implicit time variance in the <6-week-old retinopathy, globe enlarged (*rge*) chicks,[57] whereas the scotopic b-wave is supranormal with prolonged implicit times in a human cone dystrophy with a genetic mutation in the *KCNV2* potassium channel gene.[58]

While we are not certain what mechanism is responsible for the increase in the amplitudes of all the electrophysiological signals, studies by Ward et al.[59] showed an approximately 2-fold increase in the spontaneous firing of excitatory signals in RGCs following IOP elevation by microbead injection into the anterior chamber of mouse eyes compared to eyes that had been injected with saline only. The increased retinal activity was postulated to be mediated by the transient receptor potential vanilloid family of cation channels that is activated in response to IOP-associated stress.[59] The enhanced pSTR amplitudes that were observed in the present study may reflect a similar elevated IOP-induced increase in RGC electrical activity.

Nitric oxide (NO) is another possibility for a rapidly acting agent that can mediate the increase in electrophysiological signals that we observed. Vielma et al.[60] showed that low level intravitreal injections of NO donors into rat eyes were associated with increases in the amplitudes of ERG a- and b-waves, OPs and pSTRs. These enhancements were reversible, with ERG amplitudes decreasing to match those recorded before the exogenous NO injections. Nitric oxide has a role in basic physiological functions such as visual signal processing in the inner retina and in photoreceptors,[61–67] but it also has been associated with dysfunctional retinas of various mammalian species.[68–74] Several investigators have shown that chronic elevation of IOP to less than 35 mm Hg in the rat eye is associated with NO production in the retina[75,76] and the optic nerve.[76,77] An acute increase in IOP to 35 mm Hg potentially could increase NO levels, which presumably would lead to an enhancement of the electrophysiological responses. The finding that pathologic markers were not enhanced in this study following acute elevations of IOP (Figs. 6, 7) supports the idea of a physiological, rather than pathologic, response to the mechanical stress associated with a short-term moderate IOP elevation. Alternatively, pathologic changes may not have been captured, given the relatively short time course of the experiment.

We also note that should a biochemical factor be responsible for mediating the enhanced pSTR and ERG amplitudes, the factor appears to be transient. Although postloop responses were not significantly different from those before loop wear, the means were slightly higher after loop removal (Figs. 2, 3), suggesting that electrophysiological responses were collected before retinas could fully recover to their preloop physiological state. We also have observed that the pSTR amplitudes 45 to 50 minutes after loop removal, which is longer than the 30 minutes we used for this experiment, return to those of the preloop conditions (data not shown).

In summary, our results indicated measurable changes in the physiological response of retinal cells to visual stimuli during acute moderate IOP elevation using a vascular loop. Our study showed that IOP elevation to 35 mm Hg in the rat is associated with an increase in the electrophysiological response as well as a backward bowing of the ONH. The electrophysiological responses observed may have been mediated by transient biochemical factors released in response to the elevated IOP. The ability to observe changes in electrophysiological and morphologic responses with UHR-OCT might present a model for detection of moderate, fluctuating IOP elevations. Further work is required to fully understand the mechanisms involved in mediating the observed effects and whether the early detectable changes are relevant for humans.

Acknowledgments

The authors thank Nancy Gibson for helping with the perfusions and for maintaining care of the rats. Kirstie Carter helped with the anesthesia and monitoring the rats during the OCT and ERG sessions. Camilo Correa Ochoa helped with BMO depth processing. Daphne McCulloch helped with discussions about electrophysiological results and advised on analysis of data. Kristi Fung helped with the ERG data collection.

Supported by the Natural Sciences and Engineering Research Council (NSERC) of Canada Discovery Grants (VC, KB), the Ontario Research Fund (KB), the Canadian Foundation for Innovation (VC), the University of Waterloo Propel Centre Grant (VC, KB, KMJ), University of Waterloo Research Incentive Fund (KB, VC, KMJ), Joseph Ellis Family and William Black Research Funds (KMJ), VUMC Cell Imaging Shared Resource supported by Vanderbilt Vision Research Center-NIH 5P30EY008126-27 (KMJ), and Unrestricted Vanderbilt Eye Institute Departmental Grant from Research to Prevent Blindness, Inc., N.Y. (KMJ).

Disclosure: **V. Choh**, ARVO (S); **A. Gurdita**, None; **B. Tan**, None; **R.C. Prasad**, None; **K. Bizheva**, None; **K.M. Joos**, ARVO (S)

References

1. Tham Y-C, Li X, Wong TY, Quigley HA, Aung T, Cheng C-Y Global prevalence of glaucoma and projections of glaucoma burden through 2040: a systematic review and meta-analysis. *Ophthalmology*. 2014;121:2081–2090.
2. Statistics Canada. No date. *Table 105-1200 Healthy Aging Indicators, by Age Group and Sex, Household Population Aged 45 and Over, Canada and Provinces* (table). CANSIM (database). Last modified 2010-05-11. Available at: http://www5.statcan.gc.ca/cansim/pick-choisir?lang=eng&p2=33&id=1051200. Accessed August 15, 2015.
3. Buys YM, Harasymowycz P, Gaspo R, et al. Comparison of newly diagnosed ocular hypertension and open-angle glaucoma: ocular variables, risk factors, and disease severity. *J Ophthalmol*. 2012;2012:757106–757106.
4. Kwon YH, Fingert JH, Kuehn MH, Alward WLM. Primary open-angle glaucoma. *N Engl J Med*. 2009;360:1113–1124.
5. Chauhan BC, Mikelberg FS, Artes PH, et al. Canadian Glaucoma Study: 3. Impact of risk factors and intraocular pressure reduction on the rates of visual field change. *Arch Ophthalmol*. 2010;128:1249–1255.
6. Kass MA, Heuer DK, Higginbotham EJ, et al. The Ocular Hypertension Treatment Study. *Arch Ophthalmol*. 2002;120:701–712.
7. Sanchez-Parra L, Pardhan S, Buckley RJ, Parker M, Bourne RR. Diurnal intraocular pressure and the relationship with swept-source oct-derived anterior chamber dimensions in angle closure: The IMPACT Study. *Invest Ophthalmol Vis Sci*. 2015;56:2943–2949.
8. Tojo N, Oka M, Miyakoshi A, Ozaki H, Hayashi A. Comparison of fluctuations of intraocular pressure before and after

selective laser trabeculoplasty in normal-tension glaucoma patients. *J Glaucoma*. 2014;23:e138–e143.

9. Tojo N, Hayashi A, Otsuka M, Miyakoshi A. Fluctuations of the intraocular pressure in pseudoexfoliation syndrome and normal eyes measured by a contact lens sensor [published online ahead of print June 5 2015]. *J Glaucoma*.
10. Friberg TR, Weinreb RN. Ocular manifestations of gravity inversion. *JAMA*. 1985;253:1755–1757.
11. Baskaran M, Raman K, Ramani KK, Roy J, Vijaya L, Badrinath SS. Intraocular pressure changes and ocular biometry during Sirsasana (headstand posture) in yoga practitioners. *Ophthalmology*. 2006;113:1327–1332.
12. Frankfort BJ, Khan AK, Tse DY, et al. Elevated intraocular pressure causes inner retinal dysfunction before cell loss in a mouse model of experimental glaucoma. *Invest Ophthalmol Vis Sci*. 2013;54:762–770.
13. Bui BV, Edmunds B, Cioffi GA, Fortune B. The gradient of retinal functional changes during acute intraocular pressure elevation. *Invest Ophthalmol Vis Sci*. 2005;46:202–213.
14. Tsai TI, Bui BV, Vingrys AJ. Effect of acute intraocular pressure challenge on rat retinal and cortical function. *Invest Ophthalmol Vis Sci*. 2014;55:1067–1077.
15. Feghali JG, Jin JC, Odom JV. Effect of short-term intraocular pressure elevation on the rabbit electroretinogram. *Invest Ophthalmol Vis Sci*. 1991;32:2184–2189.
16. Sieving PA, Nino C. Scotopic threshold response (STR) of the human electroretinogram. *Invest Ophthalmol Vis Sci*. 1988; 29:1608–1614.
17. Perlman I. The electroretinogram: ERG. In: Kolb H, Fernandez E, Nelson R, eds. *Webvision: The Organization of the Retina and Visual System [Internet]*. Salt Lake City, UT: University of Utah Health Science Center; 2001.
18. Joos KM, Li C, Sappington RM. Morphometric changes in the rat optic nerve following short-term intermittent elevations in intraocular pressure. *Invest Ophthalmol Vis Sci*. 2010;51: 6431–6440.
19. Liu Y, McDowell CM, Zhang Z, Tebow HE, Wordinger RJ, Clark AF. Monitoring retinal morphologic and functional changes in mice following optic nerve crush. *Invest Ophthalmol Vis Sci*. 2014;55:3766–3774.
20. Zhi Z, Cepurna WO, Johnson EC, Morrison JC, Wang RK. Impact of intraocular pressure on changes of blood flow in the retina, choroid, and optic nerve head in rats investigated by optical microangiography. *Biomed Opt Exp*. 2012;3:2220–2233.
21. Zhao Y, Yu B, Xiang Y-H, et al. Changes in retinal morphology, electroretinogram and visual behavior after transient global ischemia in adult rats. *PLoS One*. 2013;8:e65555.
22. Bui BV, Fortune B. Ganglion cell contributions to the rat full-field electroretinogram. *J Physiol (Lond)*. 2004;555:153–173.
23. Moayed AA, Hariri S, Hyun C, et al. Combined optical coherence tomography and electroretinography system for in vivo simultaneous morphological and functional imaging of the rodent retina. *J Biomed Opt*. 2014;15:040506–040506.
24. Moshiri A, Gonzalez E, Tagawa K, et al. Near complete loss of retinal ganglion cells in the math5/brn3b double knockout elicits severe reductions of other cell types during retinal development. *Dev Biol*. 2008;316:214–227.
25. Saszik SM, Robson JG, Frishman LJ. The scotopic threshold response of the dark-adapted electroretinogram of the mouse. *J Physiol (Lond)*. 2002;543:899–916.
26. You Y, Gupta VK, Li JC, Al-Adawy N, Klistorner A, Graham SL. FTY720 protects retinal ganglion cells in experimental glaucoma. *Invest Ophthalmol Vis Sci*. 2014;55:3060–3066.
27. Bellezza AJ, Rintanlan CJ, Thompson HW, Downs JC, Hart RT, Burgoyne CF. Deformation of the lamina cribrosa and anterior scleral canal wall in early experimental glaucoma. *Invest Ophthalmol Vis Sci*. 2003;44:623–637.
28. Burgoyne CF, Downs JC, Bellezza AJ, Hart RT. Three-dimensional reconstruction of normal and early glaucoma monkey optic nerve head connective tissues. *Invest Ophthalmol Vis Sci*. 2004;45:4388–4399.
29. Fortune B, Yang H, Strouthidis NG, et al. The effect of acute intraocular pressure elevation on peripapillary retinal thickness, retinal nerve fiber layer thickness, and retardance. *Invest Ophthalmol Vis Sci*. 2009;50:4719–4726.
30. Quigley HA. The pathogenesis of reversible cupping in congenital glaucoma. *Am J Ophthalmol*. 1977;84:358–370.
31. Bui BV, Batcha AH, Fletcher E, Wong VHY, Fortune B. Relationship between the magnitude of intraocular pressure during an episode of acute elevation and retinal damage four weeks later in rats. *PLoS One*. 2013;8:e70513.
32. Westall CA, Dhaliwal HS, Panton CM, et al. Values of electroretinogram responses according to axial length. *Doc Ophthalmol*. 2001;102:115–130.
33. Yan DB, Coloma FM, Metheetrairut A, Trope GE, Heathcote JG, Ethier CR. Deformation of the lamina cribrosa by elevated intraocular pressure. *Br J Ophthalmol*. 1994;78:643–648.
34. Fortune B, Choe TE, Reynaud J, et al. Deformation of the rodent optic nerve head and peripapillary structures during acute intraocular pressure elevation. *Invest Ophthalmol Vis Sci*. 2011;52:6651–6661.
35. Zhao D, He Z, Vingrys AJ, Bui BV, Nguyen CT. The effect of intraocular and intracranial pressure on retinal structure and function in rats. *Physiol Rep*. 2015;3:e12507.
36. Gramlich OW, Lueckner TCS, Kriechbaum M, et al. Dynamics, alterations, and consequences of minimally invasive intraocular pressure elevation in rats. *Invest Ophthalmol Vis Sci*. 2014; 55:600–611.
37. Ivers KM, Sredar N, Patel NB, et al. In vivo changes in lamina cribrosa microarchitecture and optic nerve head structure in early experimental glaucoma. *PLoS One*. 2015;10:e0134223.
38. Deng S, Wang M, Yan Z, et al. Autophagy in retinal ganglion cells in a rhesus monkey chronic hypertensive glaucoma model. *PLoS One*. 2013;8:e77100.
39. Cuenca N, Pinilla I, Fernandez-Sanchez L, et al. Changes in the inner and outer retinal layers after acute increase of the intraocular pressure in adult albino Swiss mice. *Exp Eye Res*. 2010;91:273–285.
40. Bayer AU, Neuhardt T, May AC, et al. Retinal morphology and ERG response in the DBA/2NNia mouse model of angle-closure glaucoma. *Invest Ophthalmol Vis Sci*. 2001;42:1258–1265.
41. Fernandez-Sanchez L, de Sevilla Muller LP, Brecha NC, Cuenca N. Loss of outer retinal neurons and circuitry alterations in the DBA/2J mouse. *Invest Ophthalmol Vis Sci*. 2014;55:6059–6072.
42. Vaegan, Graham SL, Goldberg I, Buckland L, Hollows FC. Flash and pattern electroretinogram changes with optic atrophy and glaucoma. *Exp Eye Res*. 1995;60:697–706.
43. Wittstrom E, Schatz P, Lovestam-Adrian M, Ponjavic V, Bergstrom A, Andreasson S. Improved retinal function after trabeculectomy in glaucoma patients. *Graefes Arch Clin Exp Ophthalmol*. 2010;248:485–495.
44. Gur M, Zeevi YY, Bielik M, Neumann E. Changes in the oscillatory potentials of the electroretinogram in glaucoma. *Curr Eye Res*. 1987;6:457–466.
45. Holopigian K, Seiple W, Mayron C, Koty R, Lorenzo M. Electrophysiological and psychophysical flicker sensitivity in patients with primary open-angle glaucoma and ocular hypertension. *Invest Ophthalmol Vis Sci*. 1990;31:1863–1868.
46. Chen YJ, Huang YS, Chen JT, et al. Protective effects of glucosamine on oxidative-stress and ischemia/reperfusion-

induced retinal injury. *Invest Ophthalmol Vis Sci*. 2015;56: 1506–1516.

47. Heckenlively JR, Tanji T, Logani S. Retrospective study of hyperabnormal (supranormal) electroretinographic responses in 104 patients. *Trans Am Ophthalmol Soc*. 1994;92:217–231, discussion 231–233.
48. Olivier P, Jolicoeur FB, Lafond G, Drumheller AL, Brunette JR. Dose related effects of 6-OHDA on rabbit retinal dopamine concentrations and ERG B-wave amplitudes. *Brain Res Bull*. 1986;16:751–753.
49. Skrandies W, Wassle H. Dopamine and serotonin in cat retina: electroretinography and histology. *Exp Brain Res*. 1988;71: 231–240.
50. Jagadeesh JM, Lee HC, Salazar-Bookaman M. Influence of chlorpromazine on the rabbit electroretinogram. *Invest Ophthalmol Vis Sci*. 1980;19:1449–1456.
51. Schneider T, Zrenner E. Effects of D-1 and D-2 dopamine antagonists on ERG and optic nerve response of the cat. *Exp Eye Res*. 1991;52:425–430.
52. Fox DA, Kala SV, Hamilton WR, Johnson JE, O'Callaghan JP. Low-level human equivalent gestational lead exposure produces supernormal scotopic electroretinograms, increased retinal neurogenesis, and decreased retinal dopamine utilization in rats. *Environ Health Perspect*. 2008;116:618–625.
53. Rothenberg SJ, Schnaas L, Salgado-Valladares M, et al. Increased ERG a- and b-wave amplitudes in 7- to 10-year-old children resulting from prenatal lead exposure. *Invest Ophthalmol Vis Sci*. 2002;43:2036–2044.
54. Phillips MJ, Webb-Wood S, Faulkner AE, et al. Retinal function and structure in Ant1-deficient mice. *Invest Ophthalmol Vis Sci*. 2010;51:6744–6752.
55. Khan AK, Tse DY, van der Heijden ME, et al. Prolonged elevation of intraocular pressure results in retinal ganglion cell loss and abnormal retinal function in mice. *Exp Eye Res*. 2015; 130:29–37.
56. Suh M, Sauve Y, Merrells KJ, Kang JX, Ma DW. Supranormal electroretinogram in fat-1 mice with retinas enriched in docosahexaenoic acid and *n*-3 very long chain fatty acids (C24-C36). *Invest Ophthalmol Vis Sci*. 2009;50:4394–4401.
57. Montiani-Ferreira F, Shaw GC, Geller AM, Petersen-Jones SM. Electroretinographic features of the retinopathy, globe enlarged (rge) chick phenotype. *Mol Vis*. 2007;13:553–565.
58. Vincent A, Robson AG, Holder GE. Pathognomonic (diagnostic) ERGs. A review and update. *Retina*. 2013;33:5–12.
59. Ward NJ, Ho KW, Lambert WS, Weitlauf C, Calkins DJ. Absence of transient receptor potential vanilloid-1 accelerates stress-induced axonopathy in the optic projection. *J Neurosci*. 2014; 34:3161–3170.
60. Vielma A, Delgado L, Elgueta C, Osorio R, Palacios AnG, Schmachtenberg O. Nitric oxide amplifies the rat electroretinogram. *Exp Eye Res*. 2010;91:700–709.
61. Cudeiro J, Rivadulla C. Sight and insight - on the physiological role of nitric oxide in the visual system. *Trends Neurosci*. 1999;22:109–116.
62. Djamgoz MB, Sekaran S, Angotzi AR, et al. Light-adaptive role of nitric oxide in the outer retina of lower vertebrates: a brief review. *Philos Trans R Soc Lond B Biol Sci*. 2000;355:1199–1203.
63. Hoffpauir B, McMains E, Gleason E. Nitric oxide transiently converts synaptic inhibition to excitation in retinal amacrine cells. *J Neurophysiol*. 2006;95:2866–2877.
64. Mills SL, Massey SC. Differential properties of two gap junctional pathways made by AII amacrine cells. *Nature*. 1995;377:734–737.
65. Wang G-Y, Liets LC, Chalupa LM. Nitric oxide differentially modulates ON and OFF responses of retinal ganglion cells. *J Neurophysiol*. 2003;90:1304–1313.
66. Sato M, Ohtsuka T. Opposite effects of nitric oxide on rod and cone photoreceptors of rat retina in situ. *Neurosci Lett*. 2010; 473:62–66.
67. Sato M, Ohtsuka T, Stell WK. Endogenous nitric oxide enhances the light-response of cones during light-adaptation in the rat retina. *Vision Res*. 2011;51:131–137.
68. Oku H, Yamaguchi H, Sugiyama T, Kojima S, Ota M, Azuma I. Retinal toxicity of nitric oxide released by administration of a nitric oxide donor in the albino rabbit. *Invest Ophthalmol Vis Sci*. 1997;38:2540–2544.
69. Kobayashi M, Kuroiwa T, Shimokawa R, Okeda R, Tokoro T. Nitric oxide synthase expression in ischemic rat retinas. *Jpn J Ophthalmol*. 2000;44:235–244.
70. Neufeld AH, Hernadez MR, Gonzalez M. Nitric oxide synthase in the human glaucomatous optic nerve head. *Arch Ophthalmol*. 1997;1152:497–503.
71. Takahata K. Retinal neuronal death induced by intraocular administration of a nitric oxide donor and its rescue by neurotrophic factors in rats. *Invest Ophthalmol Vis Sci*. 2003; 44:1760–1766.
72. Takahata K, Katsuki H, Kume T, et al. Retinal neurotoxicity of nitric oxide donors with different half-life of nitric oxide release: involvement of N-methyl-D-aspartate receptor. *J Pharmacol Sci*. 2003;92:428–432.
73. Goldstein IM, Ostwald P, Roth S. Minireview nitric oxide: a review of its role in retinal function and disease. *Vision Res*. 1996;36:2979–2994.
74. Neufeld AH. Nitric oxide: a potential mediator of retinal ganglion cell damage in glaucoma. *Surv Ophthalmol*. 1999; 43(suppl 1):S129–S135.
75. Siu AW, Leung MCP, Ho To C, Siu FKW, Ji JZ, Fai So K. Total retinal nitric oxide production is increased in intraocular pressure-elevated rats. *Exp Eye Res*. 2002;75:401–406.
76. Vidal L, Diaz F, Villena A, Moreno M, Campos JG, de Vargas IP. Nitric oxide synthase in retina and optic nerve head of rat with increased intraocular pressure and effect of timolol. *Brain Res Bull*. 2006;70:406–413.
77. Shareef S, Sawada A, Neufeld AH. Isoforms of nitric oxide synthase in the optic nerves intraocular pressure. *Invest Ophthalmol Vis Sci*. 1999;40:2884–2891.

Investigative Ophthalmology & Visual Science